Ice in Clouds Experiment–Layer Clouds. Part II: Testing Characteristics of Heterogeneous Ice Formation in Lee Wave Clouds

P. R. FIELD,* A. J. HEYMSFIELD,+ B. J. SHIPWAY,* P. J. DEMOTT,# K. A. PRATT,@,& D. C. ROGERS,+ J. STITH,+ AND K. A. PRATHER@

* *Met Office, Exeter, United Kingdom*
+ *National Center for Atmospheric Research, Boulder, Colorado*
# *Colorado State University, Fort Collins, Colorado*
@ *University of California, San Diego, La Jolla, California*

(Manuscript received 24 January 2011, in final form 21 September 2011)

ABSTRACT

Heterogeneous ice nucleation is a source of uncertainty in models that represent ice clouds. The primary goal of the Ice in Clouds Experiment–Layer Clouds (ICE-L) field campaign was to determine if a link can be demonstrated between ice concentrations and the physical and chemical characteristics of the ambient aerosol. This study combines a 1D kinematic framework with lee wave cloud observations to infer ice nuclei (IN) concentrations that were compared to IN observations from the same flights. About 30 cloud penetrations from six flights were modeled. The temperature range of the observations was −16° to −32°C. Of the three simplified ice nucleation representations tested (deposition, evaporation freezing, and condensation/immersion droplet freezing), condensation/immersion freezing reproduced the lee wave cloud observations best. IN concentrations derived from the modeling ranged from 0.1 to 13 L^{-1} compared to 0.4 to 6 L^{-1} from an IN counter. A better correlation was found between temperature and the ratio of IN concentration to the concentration of large aerosol (>500 nm) than between IN concentration and the large aerosol concentration or temperature alone.

1. Introduction

The treatment of heterogeneous nucleation of ice is a large source of uncertainty in models of ice clouds from the highest-resolution parcel models to the coarsest-resolution climate models. The National Science Foundation funded the Ice in Clouds Experiment–Layer Clouds (ICE-L) field campaign over Wyoming and Colorado was carried out in fall 2007. The long-term goal of the project is to evaluate if the number of ice particles formed by nucleation mechanisms can be predicted when the aerosol feeding into a cloud is adequately characterized both physically and chemically. In this paper we compare aircraft observations from six flights with output from a 1D model of lee wave clouds to infer ice nuclei (IN) concentrations and consider if these estimates are consistent with direct measurements of ice nuclei concentrations.

Lee wave clouds provide an excellent natural laboratory for investigating ice nucleation mechanisms. Their relatively small physical and temporal dimensions can minimize the impact from other microphysical processes. They can potentially have the advantage of a simple laminar geometry with little turbulent mixing and be quasi-steady in time. The aerosol inputs to the cloud can be sampled upwind and passes through the cloud can be made to observe cloud properties and the dynamic and thermodynamic environment. These observations can be used to define a kinematic framework to drive a microphysical model. Potential disadvantages are that in reality some wave clouds can exhibit extensive complex structure and vary in time (Baker and Lawson 2006) that make analysis of the data challenging. Aircraft sampling is carried out along horizontal traverses that cut through individual parcel trajectories, which can make interpretation based on parcel modeling nontrivial. Natural aerosol distributions can have very heterogeneous chemical and physical characteristics.

& Current affiliation: Purdue University, West Lafayette, Indiana.

Corresponding author address: Paul Field, Met Office, Exeter EX1 3PB, United Kingdom.
E-mail: paul.field@metoffice.gov.uk

DOI: 10.1175/JAS-D-11-026.1

Previous investigations into ice nucleation through the sampling of lee wave clouds have been carried out by Cooper and Vali (1981), Heymsfield and Miloshevich (1993, 1995), Jensen et al. (1998), DeMott et al. (1998), Field et al. (2001), and Baker and Lawson (2006). These projects sampled wave clouds between −15° and −60°C. A common feature of these observations is that no ice was detected above the sensitivity of the probes (typically 0.1 L^{-1}) in the ice supersaturated region immediately upwind of the liquid wave cloud, suggesting that deposition nucleation is not a dominant mechanism for these clouds. The liquid wave cloud then becomes mixed phase at some point and is eventually replaced by an ice cloud when the liquid droplets evaporate in the downdraft part of the wave cloud. The concentrations of ice vary widely and are not a simple function of temperature (Baker and Lawson 2006). Laboratory studies have also indicated that at temperatures warmer than −35°C and colder than about −10°C the onset of ice formation on some desert dust aerosols occurs at the same time as the activation of liquid water droplets (e.g., Field et al. 2006b), while only at colder temperatures does the deposition mode become apparent (e.g., Möhler et al. 2006). Eidhammer et al. (2010) compared parcel model simulations of flight 4 from ICE-L with observations. They concluded that a condensation or immersion freezing mechanism was the most likely process forming ice. Both the parameterization of Phillips et al. (2008) relating IN number concentration to aerosol surface area and thermodynamic conditions and that of DeMott et al. (2010) relating IN number concentrations to temperature and aerosol number concentrations larger than 500 nm were good predictors of ice nuclei concentrations. Dust aerosol for that flight originated from dry lake beds located in the Great Basin region of the United States (Pratt et al. 2010b). Finally, Twohy et al. (2010) used ICE-L data to show a positive correlation between large aerosol concentrations and IN concentrations for a narrow temperature range (−29° to −24°C) with particles associated with biomass burning.

Currently, most IN measurements are made using portable detection systems based on the Continuous Flow Diffusion Chamber (CFDC) design (Rogers et al. 2001). Aerosols are exposed for 5–10 s to ice-saturated or water-saturated conditions at a predefined temperature. Mountain-top observations using the CFDC operating at warmer than −38°C and between ice and water saturation have reported 1–10 L^{-1} IN [at standard temperature and pressure (STP)] (DeMott et al. 2003a; Richardson et al. 2007) in background conditions, while higher IN number concentrations were correlated with dust episodes (Richardson et al. 2007). DeMott et al. (2003b) have reported IN number concentrations as high as 0.3 cm^{-3} for sampling within an African dust plume. Richardson et al. (2007) and Stith et al. (2009) indicated a correlation between the number concentration of aerosol larger than 300–500 nm and IN number concentration, but they note that size is unlikely to be the sole predictor of IN ability because of the important role of the aerosol chemistry. Eidhammer et al. (2009) presented a summary of CFDC measurements of IN number concentration (at STP) over a range of relative humidity values as a function of temperature indicating a general increase in IN number concentration with decreasing temperature, albeit with considerable scatter. At −35°C the IN number concentrations can reach hundreds per liter integrated over 1-min periods in situations that are highly perturbed with respect to mineral dust transports, falling off to number concentrations of about 1 L^{-1} at −10°C. More recently, DeMott et al. (2010) presented a correlation between the ratio of IN number concentration, in the condensation/immersion freezing regime, to large aerosol number concentration (size greater than 500 nm) as a function of temperature for data accumulated from several projects. They found a good correlation of IN number concentration with the large aerosol number concentrations increasing as a power law with decreasing temperature.

Deposition freezing has long been considered to be a minor contributor to ice numbers in the atmosphere (Mason 1950). Condensation or immersion freezing appears to be a more common pathway with observations in the laboratory (e.g., Field et al. 2006b; Connolly et al. 2009) and in the field from continuous flow diffusion chambers (e.g., DeMott et al. 2010) and remote sensing (Ansmann et al. 2008). Evaporation freezing is a mechanism that has been speculated about for a number of years (e.g., Rosinski and Morgan 1991; Cotton and Field 2002), but the physical basis for such a freezing mechanism is unclear. Recently Durant and Shaw (2005) demonstrated that contact freezing occurring from the inside of a droplet during evaporation could increase the freezing temperature. Additional mechanisms that may influence ice nucleation during cloud evaporation include thermophoretic affects that enhance contact freezing (Young 1974), low mass accommodation coefficients that could give rise to lowered droplet temperature relative to ambient conditions during rapid evaporation (Cooper 1995), and the precipitation of hydrated salts within a droplet during evaporation to provide an ice nucleus (Hallett 1968).

Part I in this series (Heymsfield et al. 2011, hereafter Part I) describes the instrumentation and observations from ICE-L. In this study airborne observations made with the National Science Foundation (NSF)–National Center for Atmospheric Research (NCAR) C-130 for

about 30 penetrations over six flights in lee wave clouds were used in conjunction with a 1D kinematic cloud model to derive ice nuclei concentrations. The approach used is similar to that adopted by Cotton and Field (2002).

While ice nuclei counters have a residence time of about 10 s and expansion cloud chambers have residence times of about 100 s, the residence time of lee wave clouds can be even longer (200–800 s in these clouds). Combining aircraft observations in lee wave clouds and 1D cloud modeling forms an independent method of inferring IN concentrations and can be viewed as an alternative IN counter.

2. Instrumentation and data treatment

Part I describes and evaluates key instrumentation used in ICE-L. Here a brief description of the subset of instrumentation used is provided. Instrumentation included a new NCAR-developed fast 2D-C probe (64 elements, 25-μm pixel size, improved response time) based on the architecture and sampling methodology of standard optical array probes (Knollenberg 1970). Processing of the 2D-C data (see Field et al. 2006a) included interarrival time filtering to remove shattering artifacts, but the narrow nature of the ice particle size distributions in lee wave clouds meant that shattering effects were minimal. For the flight data used here the fraction of particles with interarrival times indicative of particles shattering on the ice probe housing and giving rise to false signals was on average roughly less than 15% for all of the sampling legs used. This value was less for flight 3 and not possible to determine for the penetrations used in flight 4 because of the low numbers of particles counted. Flight 6 was slightly worse with an average false signal contribution of about 20%. Comparisons between the 2D-S and fast 2D-C showed good agreement (Part I). However, only the 2D-C data were available for all of the flight data used in this paper and so we concentrate on data from that instrument. To reduce problems with concentration accuracy, analysis of the 2D-C data has been restricted to particles larger than a threshold size. This was chosen to be 125 μm based on previous work (e.g., Strapp et al. 2001). This will likely underestimate the total number concentration of ice, but we will be comparing ice concentrations from the model using the same size threshold. Droplets concentrations were measured with a cloud droplet probe (CDP; 3–43 μm, Droplet Measurement Technologies).

Bulk and environmental probes included the Rosemount Icing Detector (RICE), King liquid water probe (LWP), and the tunable diode laser hygrometer (TDL). The TDL humidity measurement was corrected according to the method described in Part I. Additionally the time series for each run was subject to another small multiplicative correction (on the order of 1%) to ensure that the relative humidity was at water saturation when the King liquid water content (LWC) probe detected greater than 0.02 g m^{-3}. Other core measurements of winds and temperature were also recorded.

Aerosol characterization instrumentation included an Ultra High Sensitivity Aerosol Spectrometer for size-resolved number concentrations (UHSAS 100 nm–1 μm, Droplet Measurement Technologies, United States). Because of the small number of particles detected for aerosols larger than 500 nm, the values have been aggregated over the duration of the out-of-cloud portions of flight legs between the equivalent potential temperature ranges covered by the cloud penetrations used in the model simulations. Out-of-cloud regions were defined as where the integrated 2D-C ice water content (IWC) was less than 10^{-5} g m^{-3}, the CDP measured concentration was less than 0.01 cm^{-3}, and King liquid water content was less than 0.02 g m^{-3}.

A continuous flow diffusion chamber (CFDC; IN counter) was used to measure ice nuclei concentrations (Rogers et al. 2001; Eidhammer et al. 2010), either from ambient aerosol or using counterflow virtual impactor (CVI) residuals. Ambient sampling was from the Wyoming heated inlet, a flow-through inlet with a diffusing nozzle upstream, a converging nozzle downstream, and a calculated collection efficiency of approximately 75% for 1-μm-diameter particles when operated at typical C-130 sampling air speeds ($\sim$150 m s^{-1}). The CVI (Twohy et al. 1997) typically sampled cloud particles having diameters above about 7 μm. A preimpactor between the aircraft inlets and the CFDC removed particles with aerodynamic diameters larger than 1.5 μm to prevent false counting of any such particles as activated ice crystals. The aerosol was then exposed for 5–10 s at a predetermined humidity (supersaturated with respect to ice) and temperature before being exposed for a short time to conditions below water saturation to remove any droplets. The remaining particles were measured by an optical particle counter. Particles larger than 2 μm are classified as ice particles and provide a direct measure of the IN concentration. This excluded assessment of IN contributions from these larger particles (>2 μm). Sample volumes are low (1 L min^{-1}) but are enhanced when sampling from the CVI. Out-of-cloud concentrations are presented in this paper. The size and chemistry of individual particles and CVI cloud residues (70–1200-nm vacuum aerodynamic diameter) were measured in real time using the aircraft aerosol time-of-flight mass spectrometer (A-ATOFMS) (Pratt et al. 2009). Additional details concerning the effect of the CVI location on sampling are discussed in Part I.

From six flights made in lee wave clouds (rf03, 17 November 2007; rf04, 18 November 2007; rf06, 29 November 2007; rf09, 10 December 2007; rf11, 13 December 2007; rf12, 16 December 2007) a subset was created to use in conjunction with a 1D model. Penetrations that exhibited vertical velocities with peak magnitudes greater than 0.2 m s^{-1}, had an aircraft heading within 45° of the mean wind direction, had an absence of cloud at the upwind end of the sampling leg, and were moist enough to exceed ice saturation were included. This resulted in about 30 runs covering a temperature range of −16° to −32°C being used in the analysis (note that model parcel trajectories can go to colder temperatures than this).

All of the time series of observations (1-Hz data) were converted to air parcel time through the cloud by multiplying the observation time by the ratio of ground speed along the wind direction to wind speed. This was the time base used in the modeling and for comparing with the observations.

3. Modeling approach

a. Dynamics and microphysics

The model framework used was a simple 1D framework. The Kinematic Dynamical (KiD) model was developed as a 1D kinematic driver to aid the comparison and understanding of different microphysics parameterizations [for details, see Shipway and Hill (2012)]. The advection scheme in the KiD is the Total Variance Diminishing (TVD) scheme of Leonard et al. (1993), known as ULTIMATE. The ULTIMATE scheme is a monotonicity-preserving scheme in one-dimensional flows and is employed as one of the main advection schemes in the Met Office Large Eddy Model (LEM). A time step of 0.5 s and a vertical resolution of 15 m were chosen.

This dynamical framework was used to drive the three-phase multispecies microphysics representation (Swann 1998) from the Met Office LEM. The model represents water vapor, cloud liquid water (mass only), rainwater (mass), cloud ice (mass and number), snow (mass and number), graupel (mass and number), and the processes that convert between them. For modeling the lee wave clouds only cloud liquid and cloud ice were considered. The treatment of cloud liquid is very simple: any vapor mixing ratio in excess of liquid saturation is condensed out into liquid and divided among a predefined droplet concentration consistent with the in situ measurements of droplets (~100 cm^{-3}). Ice was assumed to have an exponential size distribution. For ice particles Part I shows that the inferred mean effective density (defined as the density of a sphere just enclosing a particle) of the ice varies from 100 kg m^{-3} for a particle with a maximum dimension of 100 μm to 50 kg m^{-3} for 200-μm particles and then decreases further for larger particles. Those results showed variability in density of up to a factor of 3 that was attributed to variations in habit. Extrapolating the trend in effective density presented in Part I (see Fig. 18 of Part I) to smaller sizes would lead to effective densities exceeding that of solid ice at about 40 μm. Inspection of imagery presented in Part I (Fig. 12, RF12 panel) reveals a small 60-μm column that has an aspect ratio of 2:1. If such a particle was completely solid it would have an effective density of about 0.2 kg m^{-3}. Part I also reviews previous laboratory work (Ryan et al. 1976; Takahashi et al. 1991) and shows that particles grown at water saturation at similar temperatures to those sampled in ICE-L have effective densities of 100 kg m^{-3} for crystal sizes down to 50 μm (Fig. 1 of Part I). Given the scatter in inferred effective density and the narrow size range of the crystals encountered (mass-weighted mean sizes generally smaller than 300 μm), a constant effective ice density of 100 kg m^{-3} was used. Using a constant density also avoids potentially anomalously high effective densities for small crystals. Sensitivity to this choice is discussed later in the paper.

Homogeneous droplet freezing was set to occur at temperatures colder than −37°C. This is a simplified approach where all cloud droplets colder than this threshold temperature immediately freeze.

b. Constructing the initial profile

For each simulation an ''initial'' vertical profile of potential temperature and total water is required. When the aircraft flies along the wind direction through a lee wave cloud it cuts through streamlines. Therefore it can be seen that if the geometry of the streamline is known then a parcel of air sampled by the aircraft could be traced back in time to a point upstream that will usually not be at the same altitude as the aircraft. Using this method, it is possible to construct a vertical profile of these parcels at a location upstream of the lee wave cloud for all of the aircraft observations. To generate vertical profiles of potential temperature and total water two assumptions were adopted. The first was that the horizontal profile of vertical velocity and the mean horizontal wind measured by the aircraft for each penetration were the same for all altitudes above and below the aircraft. The second assumption was that for a lee wave the total water and liquid potential temperature would be conserved along stream lines defined by the wind measurements. Therefore, given the vertical and horizontal wind, parcels can be traced back along stream lines to the furthest upwind point of the aircraft observations to form initial vertical profiles of temperature and humidity.

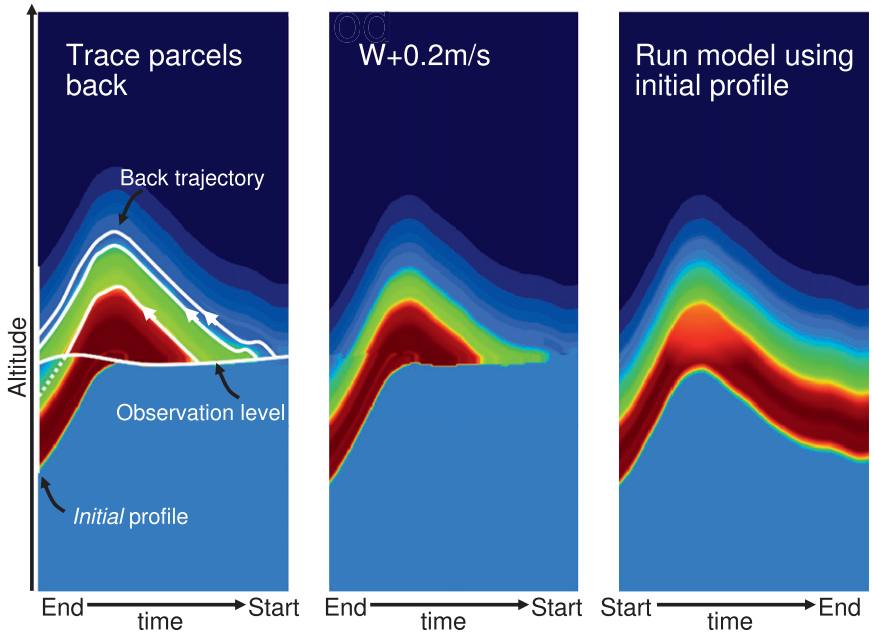

FIG. 1. Schematic of modeling approach for deriving the initial thermodynamic profile for each model run. (left) Tracing parcel trajectories backward without microphysics; total water trajectories. (middle) As at left, but with a $+0.2$ m s^{-1} change to vertical velocity field. (right) Running the model forward with microphysics on, showing water vapor trajectories. The color shading indicates the total water or water vapor amount.

To form the initial thermodynamic profile we needed to advect the parcels backward in time using our model. To track the parcels backward along the streamlines, the observed time series of humidity, condensed water, potential temperature, and vertical velocity were reversed. Additionally, the reversed vertical velocity was also inverted. Now, running the model (without the microphysics acting) advects parcels backward in time. If a parcel recrossed the flight track the observation of humidity and potential temperature superseded the original one.

Figure 1 shows an example of the total water field when the parcels were traced backward. From this run it can be seen that there is a discontinuity in the advected field. To remedy this situation and provide a more consistent initialization profile, a small offset was added to the observed vertical velocity (a difficult quantity to measure accurately). In this case it was 0.2 m s^{-1}. The absolute accuracy of the vertical wind measured from an aircraft is limited by the accuracy at which the aircraft angle of attack and height above ground is known. Typically this would result in a systematic error on the order of tenths of a meter per second. Additional errors could also arise from supercooled liquid water affecting the measurements of the pitot ports used to estimate vertical velocity. While these effects cannot be proven to have been acting, the addition of a small offset to the vertical velocity field of each penetration (see Table 1) does provide much more consistent initial profiles (Fig. 1, middle panel).

The initial profile of potential temperature and total water for each penetration was then run forward with the microphysics acting for three different freezing representations and different parameter settings that controlled the IN number concentrations. The results of the simulations were then compared to the observations.

c. *Treatment of ice nucleation*

The singular description of ice nucleation assumes that ice nuclei become active at well-defined temperatures (or relative humidities for deposition nucleation). Ice formation only occurs when the candidate nuclei are exposed to decreasing temperatures (or increasing relative humidity) (e.g., Connolly et al. 2009; Möhler et al. 2006). No new ice is formed if the temperature (or humidity) is held constant. The stochastic description is based on the probability of ice embryos forming by fluctuations in the water substance catalyzed by the presence of nuclei. This description results in a temperature-dependent nucleation rate. The number concentration of ice formed is a function of time when the stochastic description is used. Experiments where particles were suspended in supercooled droplets at fixed temperatures

TABLE 1. Derived IN (range based on temperature range) and N_{in0} concentrations from the results of the lee wave cloud modeling a threshold ice crystal size of 125 μm. These are tabulated for $B = 0.2$ in Eq. (1). Flight average UHSAS concentrations for aerosol particles in the size range 0.5–1 μm and the 2 $\times$ sigma bounds based on the Poisson sampling error. The 95th percentile measured ice concentrations (1 Hz) for particles larger than 125 μm is given. Also listed are the research flight, the times of the cloud penetration ("Start" and "End" columns, in seconds past 0000 UTC), and the temperature range of the heterogeneous freezing events for each penetration (ignores homogeneous freezing events). The numbers in parentheses represent the cloud number and penetration number for reference. The asterisks indicate if the data were used in Fig. 5. The equals sign indicates if the model produces liquid water colder than −34°C.

Flight	Start	End	UHSAS (cm^{-3})			Ice concentration (L^{-1})	T range (°C)	IN concentration (L^{-1})		w offset ($m\ s^{-1}$)
			Mean	-2σ	$+2\sigma$			N_{in0}	IN range	
3 (2, 1)*	74 538	74 945	0.11	0.09	0.14	20.2=	−31.9, −22.4	6.0	2.2, 0.3	+0.2
3 (2, 3)*	75 544	75 941	0.11	0.09	0.14	87.4=	−32.8, −24.4	6.0	2.6, 0.5	+0.8
3 (2, 5)*	76 563	76 923	0.11	0.09	0.14	28.6=	−33.9, −29.2	6.0	3.3, 1.3	+0.4
3 (2, 6)*	77 096	77 253	0.11	0.09	0.14	6.6	−32.8, −31.9	30.0	12.9, 10.8	+0.0
3 (2, 7)*	77 675	77 763	0.11	0.09	0.14	45.8=	−34.7, −31.4	10.0	6.3, 3.3	+0.0
4 (1, 3)	74 175	74 325	0.01	0.01	0.02	0.4	−32.0, −28.0	1.0	0.4, 0.2	+0.0
4 (1, 4)	74 589	74 750	0.01	0.01	0.02	0.3	−31.8, −28.4	0.6	0.2, 0.1	−0.3
4 (1, 5)	75 000	75 130	0.01	0.01	0.02	0.3	−33.0, −27.7	0.6	0.3, 0.1	+0.3
4 (1, 6)	75 767	75 940	0.01	0.01	0.02	0.3	−30.7, −29.8	3.0	0.9, 0.7	+0.4
4 (2, 2)*	79 279	79 465	0.01	0.01	0.02	0.5	−30.3, −27.2	3.0	0.8, 0.4	−0.4
4 (2, 3)	79 617	79 835	0.01	0.01	0.02	0.5	−29.6, −26.4	1.0	0.2, 0.1	+0.1
4 (2, 4)	80 054	80 199	0.01	0.01	0.02	0.2	−29.5, −26.4	1.0	0.2, 0.1	−0.1
4 (2, 5)	80 500	80 662	0.01	0.01	0.02	0.4	−31.6, −27.1	1.0	0.3, 0.1	+0.1
4 (2, 6)*	80 997	81 147	0.01	0.01	0.02	0.6	−31.1, −26.7	1.0	0.3, 0.1	−0.1
4 (2, 7)*	81 762	81 946	0.01	0.01	0.02	1.2	−31.2, −25.7	1.0	0.3, 0.1	+0.5
6 (2, 1)*	66 951	67 071	0.08	0.06	0.10	17.4	−31.1, −23.5	6.0	1.8, 0.4	−0.3
6 (2, 2)	67 414	67 543	0.08	0.06	0.10	4.4=	−33.2, −26.3	3.0	1.4, 0.3	+0.0
9 (1, 2)*	65 364	65 557	0.48	0.32	0.65	6.5	−26.8, −23.8	30.0	3.9, 2.2	+0.0
9 (1, 3)*	65 709	65 839	0.48	0.32	0.65	4.7	−26.2, −24.8	10.0	1.1, 0.9	+0.2
11 (1, 3)*	61 146	61 257	0.13	0.12	0.15	0.9=	−25.6, −16.8	3.0	0.3, 0.1	−0.3
11 (1, 4)	61 309	61 369	0.13	0.12	0.15	0.5	−23.1, −17.4	6.0	0.4, 0.1	+0.3
11 (2, 1)*	67 690	67 773	0.13	0.12	0.15	3.9	−25.9, −20.9	6.0	0.7, 0.2	−0.2
11 (2, 5)*	68 969	68 986	0.13	0.12	0.15	2.3	−20.8, −16.0	30.0	1.2, 0.4	−0.2
12 (2, 2)*	69 086	69 229	0.71	0.66	0.15	5.5	−27.5, −24.0	30.0	4.5, 2.2	+0.25
12 (2, 3)*	66 038	66 241	0.71	0.66	0.76	6.3	−26.3, −24.6	100.0	11.8, 8.3	+0.0
12 (2, 4)*	66 340	66 505	0.71	0.66	0.76	3.4	−25.5, −24.5	10.0	1.0, 0.8	+0.5
12 (2, 7)*	66 691	66 960	0.71	0.66	0.76	1.0	−25.5, −24.5	6.0	0.6, 0.5	+0.2
12 (2, 8)*	67 891	68 036	0.71	0.66	0.76	1.8	−25.0, −24.0	10.0	0.9, 0.7	−0.1

were observed to freeze over time, providing evidence for a stochastic immersion freezing mechanism (e.g., Murray et al. 2011, using kaolinite). Vali (1994, using soil samples) also observed time-dependent freezing but an exponential decay of freezing rates with time at constant temperature. Vali (1994) also noted that during steady cooling a singular approach was adequate and when cooling was halted the number concentration of ice was only likely to double after long time intervals. Other work such, as that by Connolly et al. (2009), has successfully used a singular description of ice nucleation to represent the laboratory cloud chamber observations.

The controversy concerning whether stochastic or singular approaches best represent heterogeneous ice nucleation has been revisited by Niedermeier et al. (2011). They attempted to resolve the apparent contradiction in laboratory studies by proposing a conceptual model based on surface site heterogeneity. This model predicts an approximately singular freezing behavior to arise for broad size distributions with heterogeneous surface properties that are individually treated in a stochastic manner. Indeed, it is recommended that in order to assess the full ice nucleating characteristics of an aerosol population, the particle size distribution should be as narrow as possible and the surface properties should be uniform. This is challenging for aircraft measurements where the aerosol population is heterogeneous and varies from flight to flight. In the lee wave cloud air parcels are subject to a cooling rate that reduces to zero at the wave crest but then reverses as the parcel descends, leading to warming. There are no periods when the temperature is held stationary. Even when the thermodynamic environment can be controlled and the aerosol population is well characterized it is noted that laboratory studies are able to satisfactorily fit the observations using either a stochastic or singular approach (e.g., Murray et al. 2011).

The approach adopted here is to trial simplified distinct representations of ice formation that capture some of the essence of different heterogeneous freezing processes. We do not attempt to tackle the issue of whether stochastic or singular is more appropriate. The approach used will identify characteristics of ice formation that would be beneficial for a heterogeneous ice nucleation parameterization to possess. Furthermore, the form of the IN concentration dependence on temperature (or relative humidity) is based on reference to the empirical studies rather than an activation spectra approach. This choice reduces the number of unknowns that need to be determined.

For the comparison with the aircraft data the following assumptions taken together have been made:

- The singular hypothesis for heterogeneous ice nucleation is adopted. If a sample of aerosol immersed in supercooled droplets is cooled then more ice particles will immediately form. If a sample is held at a constant temperature then no new ice particles are formed. An analogous approach for supersaturation with respect to ice was adopted for deposition nucleation.
- Three simplified representations are tested independently: (i) condensation/immersion freezing, (ii) deposition nucleation, and (iii) evaporation freezing. Condensation/immersion droplet freezing depleted the IN reservoir when supercooled droplets were present. Deposition nucleation occurred when the relative humidity was between 2% supersaturation with respect to ice and water saturation. Evaporation freezing occurred when droplets were evaporating and the vertical velocity was negative (downward).
- For condensation/immersion and evaporation freezing the number of ice particles formed from droplets is determined by an exponential function of temperature. The IN available for ice formation via condensation and evaporation were controlled by the following temperature-dependent function that makes more IN available at colder temperatures:

$$N_{\text{in}}(T) = N_{\text{in0}} \exp(-BT^*), \tag{1}$$

where $N_{\text{in}}(T)$ is the available IN concentration at temperature T, N_{in0} is the maximum available IN number concentration at −37°C (at temperatures colder than this $N_{\text{in}} = N_{\text{in0}}$), and T^* is temperature variable ($T + 37.0$; °C). IN are carried as a prognostic field initially populated with a number density of N_{in0}. As the temperature decreases ice are immediately formed according to Eq. (1), and consequently the IN prognostic field is depleted by the same amount. Subsequent increases in temperature will not affect the ice or IN number concentration. Carrying the IN as a separate prognostic variable allows the thermodynamic history of air entering the lee wave cloud to be tracked. If sedimentation of ice depletes a parcel of ice number then new ice will not be formed unless the parcel becomes colder than it has been in the past. Inspection of the literature suggests a value for B of 0.2–0.3 (e.g., Eidhammer et al. 2009; Cooper 1986). We have chosen $B = 0.2$ and also looked at the effect of choosing 0.4.

- For deposition nucleation the number of ice formed is determined by an exponential function of ice supersaturation:

$$N_{\text{in}}(T) = N_{\text{in0}} \exp(CS^*), \tag{2}$$

where N_{in0} is now the maximum available IN number concentration at water saturation and S^* is the ice supersaturation variable ($e/E_i - E_w/E_i$), where e is the water vapor pressure and E_i and E_w are the saturation vapor pressure over ice and water, respectively (S^* is zero at water saturation and negative below water saturation). Deposition nucleation acted when the relative humidity exceeded 2% supersaturation with respect to ice and was less than water saturation. Again, inspection of the literature suggests a value of 10 for C (e.g., Meyers et al. 1992).

The freezing representations used fixed maximum IN concentrations (N_{in0}) in terms of number per unit volume of ambient air ranging from 1 to 10^6 m^{-3} in steps (1, 3, 6, 10, 30, 60, 100, . . .). By comparing the results of trialing these freezing representations using each value of N_{in0}, with metrics derived from observed cloud properties, the best solutions were chosen.

d. Metrics

Two metrics were used to compare the observations against the model output. We are interested in ice particle concentration greater than a threshold size and the time for the ice crystals to grow past that size because they are thought to be accurately measured. Therefore, only metrics concentrating on these aspects were considered. The metrics were derived from the observations and model output at the level of the aircraft observation. The first metric (Fig. 2, top) is defined as

$$m_1 = \sum \log_{10}[N_i(D > 125\,\mu\text{m}, N_i > N_{\text{th}})/N_{\text{th}}]\delta t, \tag{3}$$

where N_{th} is a threshold concentration (100 m^{-3}) and δt is the sample interval. This threshold is quite small, but the metric is cumulative, so only penetrations with more

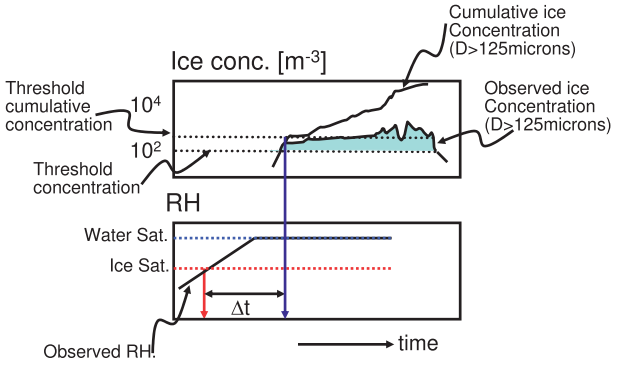

FIG. 2. (top) Schematic of ice concentration metric. This is the sample interval multiplied by the sum of logarithm of the ratio of ice concentration to a threshold concentration measured for particles greater than 125 μm along the flight track. (bottom) Schematic of the time to first ice metric. This is the time between ice saturation being reached and the observation (model simulation) of cumulative ice concentrations greater than 1000 m^{-3} for ice crystals larger than 125 μm ($\Delta t_{obs,model}$).

than 10 ice concentration samples above this threshold were used. This metric can be viewed as a measure of ice concentration path. By using the logarithm of the concentration the problem of the greater concentrations near the downwind side of the cloud dominating any metric is avoided. For each freezing mechanism the best-fit N_{in0} value was identified by examining the ratio of the observed ice concentration path metric m_1 to the model-derived version. The N_{in0} value that produced the closest model ice concentration path metric value to the observed value was chosen as the solution. Other size thresholds were also used for this metric to assess whether the choice of ice particle density was appropriate.

The second metric (Fig. 2, bottom) is a measure of the time until the first ice larger than 125 μm is observed. It is defined as the parcel time between when ice saturation is reached and the first cumulative ice concentrations exceed 1000 m^{-3} for particles larger than 125 μm ($\Delta t_{obs,model}$). Ratios of the time to first ice metric were examined to determine which mechanisms produced the closest match to observations.

4. Results

Figure 3 shows a height–time contour plot of modeled liquid and ice water contents (derived by integrating the 2D-C size distribution and assuming an effective ice density of 100 kg m^{-3}) for one of the penetrations [RF12, cloud 2, penetration 2: 12 (2, 2)] as well as modeled and observed values of different variables at the level of aircraft observation. Results for the three freezing representations are shown that produced the best match to the metrics. In all cases the liquid water and relative humidity are well reproduced (not all shown), validating the methodology used to initialize the simulation. The condensation simulation shows good agreement with the ice number concentration and ice water content. This simulation used an N_{in0} number concentration of 30 L^{-1}, which results in IN number concentrations of 2–4 L^{-1} for the temperature range modeled. The evaporation freezing representation (using a N_{in0} concentration of 60 L^{-1}, leading to IN concentrations of 4–9 L^{-1}) is unable to match the observed ice concentration profile early on in the cloud. Just considering this pass alone, it is clear that evaporation freezing acting in isolation is not sufficient to reproduce the observed ice signal. The earlier than observed onset of ice produced by deposition (using an N_{in0} concentration of 3 L^{-1}, leading to IN concentrations of 0.5–2 L^{-1}) appears to be a method of discriminating between whether deposition or droplet freezing produces a solution that compares better with the observations.

Using the ice concentration path metric [Eq. (3)] the best model-derived N_{in0} concentration for each freezing representation was determined. Figure 4 shows the typical monotonic behavior of the model to observed ratio of this metric as a function of N_{in0} concentration used in the model simulation. The model N_{in0} concentration that produced the best match to this metric for the observed value was chosen as the best estimate. For these solutions the elapsed time between the appearance of ice above a given size threshold (125 μm), a cumulative concentration of 1000 m^{-3}, and the relative humidity reaching ice saturation are determined. Figure 5 shows the ratio of the elapsed time from the model Δt_{model} and the observations Δt_{obs} for each penetration from all of the flights where the 95th percentile of the measured ice concentration (to avoid potential spikes that using the maximum concentration might introduce) exceeded 500 m^{-3}. A value of one means that the model elapsed time between reaching ice saturation and the appearance of ice matches the observation. It is clear that the results for condensation/immersion droplet freezing are generally closer to one than for the deposition and evaporation representations. The generation of ice through deposition nucleation is consistently early ($\Delta t_{model}/\Delta t_{obs} < 1$), while ice from evaporation freezing appears consistently late ($\Delta t_{model}/\Delta t_{obs} > 1$). From Fig. 5 it is concluded that if only one freezing representation is acting then a process that forms ice coincident with the occurrence of droplets (condensation/immersion droplet freezing) produces the best timing in terms of delay between ice saturation and the onset of observable ice.

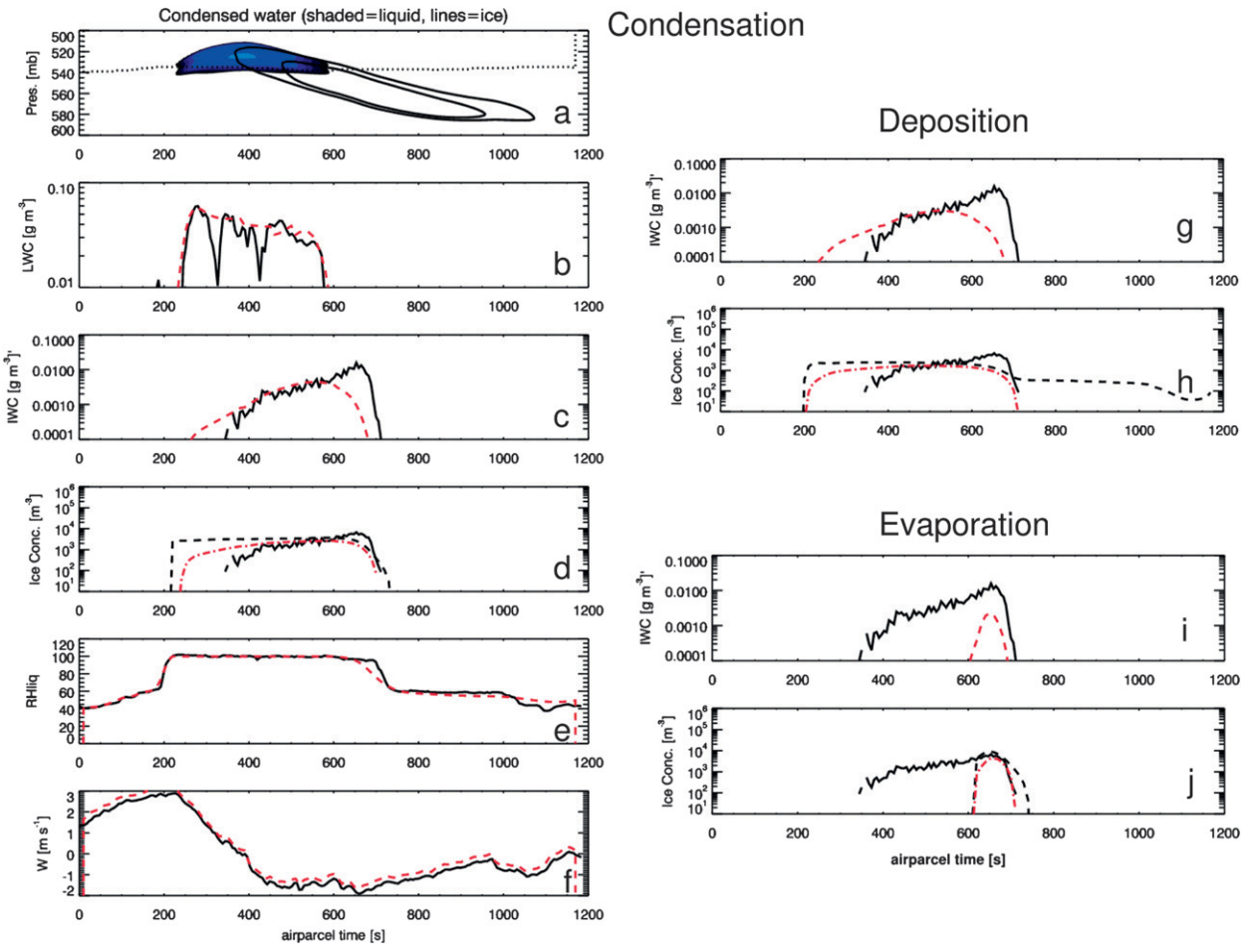

FIG. 3. Example observations and results for modeling of one lee wave cloud penetration from research flight 12. (a)–(f) Results for condensation freezing ($B = 0.2$) and an N_{in0} concentration of 30 L^{-1}. (a) Condensed liquid and ice water contents as a function of pressure and air parcel time. The dotted line shows the aircraft sampling altitude along which the model output has been sampled to compare with the observations. (b) Liquid water content (black solid is King LWC; red dashed is modeled LWC) (c) Ice water content (black solid is integrated 2D-C assuming spherical ice with constant 0.1 g cm^{-3} density; red dashed is modeled). (d) Ice concentration (black solid is 2D-C sizes > 125 μm; black dashed is modeled total concentration; red dot-dashed is modeled concentration for particles > 125 μm). (e) Relative humidity with respect to liquid (black solid is observed; red dashed is modeled). (f) Vertical velocity (black solid is observed; red dashed is modeled including slight offset). (g)–(j) As in (c),(d), but for deposition with an N_{in0} concentrations of (g),(h) 3 and (i),(j) 60 L^{-1}.

As an additional caveat, we note that if deposition freezing had an onset relative humidity threshold close to water saturation it would be difficult to determine whether freezing was due to deposition or a condensation mechanism. For the temperatures encountered in this study the humidity threshold would need to be about 20%–30% supersaturation with respect to ice to be close to water saturation. For the remaining plots the model-derived IN concentrations for condensation freezing only will be considered. Model-derived IN concentrations are given in Table 1.

As a model sensitivity analysis the effect of using different size thresholds and effective ice density on the N_{in0} concentration results were examined. Ideally, the best solution for each model run should be insensitive to the choice of size threshold used to generate the metric given in Eq. (3). For an assumed effective ice density of 100 kg m^{-3} the effect on the computation of m_1 by changing size thresholds from 125 to 75 μm or 125 to 175 μm led to the same solution in about 80% of the cases where the larger threshold gave a solution. For the cases that did not agree, the solution was the adjacent value trialed (i.e., a factor of 2–3 different). For an effective ice density of 500 kg m^{-3}, the agreement ratio for changing the size thresholds was reduced to about 40%. Therefore, using an effective ice density of 100 kg m^{-3} provided a result that was more independent of size threshold chosen for measuring the concentration of ice

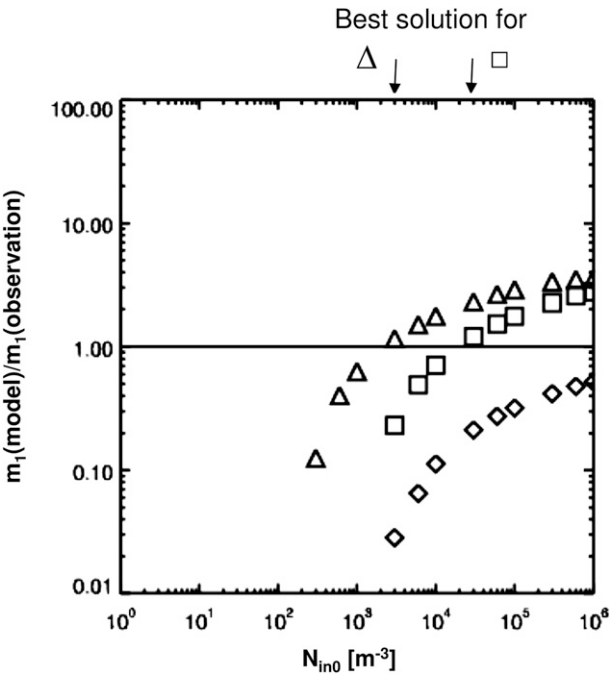

FIG. 4. Example of the behavior of the ratio of the modeled and observed ice concentration path metric for one of the lee wave cloud penetrations in flight 12 [12 (2, 2); Table 1] as a function of N_{in0} concentration. Symbols: diamond–evaporation, triangles–deposition (best solution = 3000 m^{-3}), squares–condensation (best solution = 3×10^4 m^{-3}).

and consistent with the range of low densities reported in Part I.

Scatterplots of model-derived IN concentration against temperature or large-aerosol (1000 nm $> D >$ 500 nm) concentrations only show limited correlations (not shown). Much better correlations are seen between the ratio of model-derived IN concentration and large-aerosol (1000 nm $> D >$ 500 nm, where 1000 nm is the large size limit of the UHSAS) number concentration versus temperature (Fig. 6). We note that the total surface area of these large aerosols (assuming spherical geometry) is correlated well with the concentration and is adequately approximated by simply multiplying the concentration by the surface area of a 500-nm sphere. These results suggest that larger aerosols are more efficient as IN, that their number concentrations predict the number concentrations of IN, and that IN efficiency increases with decreasing temperature. The temperature range indicated in Fig. 6 (and Table 1) is determined from the warmest and coldest temperatures for which heterogeneous freezing occurs in each model run. Results from different simulations appear consistent with the exponential dependence on temperature from Eq. (1) and the choice of $B = 0.2$ in Eq. (1) appears adequate.

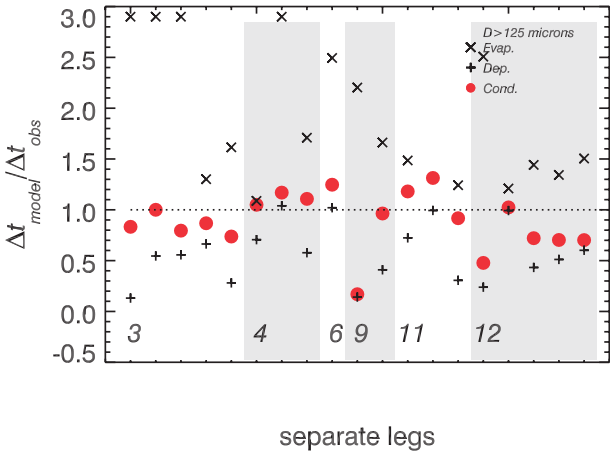

FIG. 5. Time until first ice metric. Ratio of the time between ice saturation and the observation of cumulative concentrations greater than 1000 m^{-3} for particles larger than 125 μm. Results from each cloud penetration are presented in vertical columns and each flight has alternately shaded backgrounds. The symbols closest to 1 show the closest match to the observations. Values less (greater) than 1 indicate that the model formed ice earlier (later) than the observations suggest. Ratios exceeding 3.0 were plotted at 2.9 to include them in the plot.

5. Discussion and summary

Determination of IN concentration using a model combined with observations of path-integrated ice crystal concentrations provides a more robust estimate than simply taking the maximum measured ice concentration to represent the IN concentration. This is because the

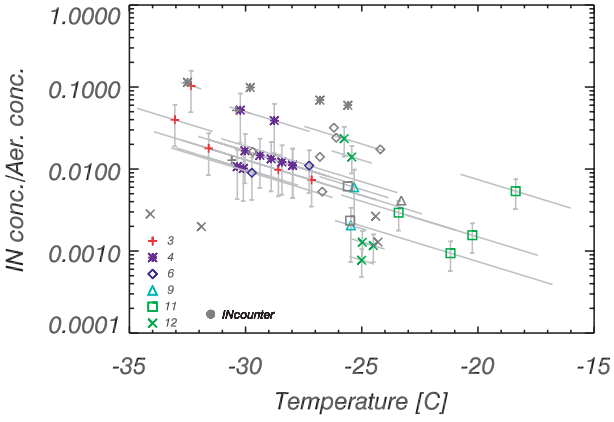

FIG. 6. Fraction of aerosol between 500 nm and 1 μm acting as ice nuclei as a function of temperature from condensation freezing. Vertical error bars are based on the resolution of the IN trials (one-third of a decade) and the temperature range is defined by the temperature at which freezing occurred during the model run. The angle of line is determined by Eq. (1) with $B = 0.2$. These results are derived from using ice particles larger than 125 μm. The gray symbols are derived from IN concentration measurements made with the IN counter.

model allows us to restrict comparisons to observations that are believed to be more accurate and include interactions between different processes. First, there is some uncertainty about the size threshold that should be used for ice crystal concentration to ensure that as many as possible are counted without including artifacts due to detection problems and uncertainties in sample volume corrections for small particles. This is an instrument issue, but by restricting comparisons between the model and observations to size ranges where the measurements are more accurate, results will be improved. Second, ice produced from homogeneous freezing at colder levels above the observation level can follow trajectories into the observation level, introducing high concentrations of ice and hence incorrectly implying high IN concentrations. The model is able to simulate when this kind of complex behavior is occurring, so it is possible to flag those penetrations and still derive an estimate of the heterogeneous IN population that satisfies the observations.

To highlight the potential shortcomings of using measured ice concentration as an estimate of IN concentration Table 1 shows 95th percentiles of 2D-C measured ice concentration (1 Hz) using the 125-μm size threshold to determine the ice concentration and model-derived IN concentrations. For flight 3 and some of flight 6 it can be seen that the measured ice concentrations are generally an order of magnitude greater than the model-derived IN concentrations. This is probably due to the influence of homogeneous freezing on these runs (indicated measurements are where the model predicted liquid water colder than −34°C). When homogeneous freezing was not active, the concentrations (95th percentile, 1-Hz data) of ice greater than 125 μm ranged from 0.2 to 17 L^{-1}.

Ice formation through a condensation/immersion droplet freezing representation appears to provide a better fit to observations than the deposition nucleation or evaporation freezing alone. While it is not possible to completely rule out the action of these other representations, if deposition nucleation is acting it appears that concentrations of IN acting in this mode are not greater than 0.1 L^{-1}. We have employed simple representations that capture some of the properties of the ice nucleation modes. The conclusions that can be drawn relate to the characteristics that are represented. Hence, the success of the condensation/immersion freezing results suggests that a process that produces ice coincident with the onset of droplet formation would be a beneficial property of an ice nucleation parameterization. Because we have taken a simplified approach to representing ice nucleation it is possible that the inclusion of increased complexity such as time dependency in the treatment of heterogeneous ice nucleation could impact this conclusion.

TABLE 2. Average out-of-cloud IN counter data from ICE-L for aerosol exposed to water saturation conditions (100.5%–103.8% RH with respect to water).

Flight	Temperature (°C)	IN concentration (L^{-1})
3	−30.4	5.7
3	−30.6	1.4
4	−32.5	1.1
4	−29.8	1.0
4	−26.8	0.7
4	−25.6	0.6
6	−29.7	1.3
6	−26.7	0.4
6	−26.8	1.1
6	−26.1	1.9
6	−26.2	2.6
6	−24.2	1.4
9	−23.3	2.0
11	−25.5	0.3
11	−25.6	0.8
12	−34.1	2.0
12	−31.9	1.4
12	−24.3	0.9
12	−24.4	1.9

The results shown in Fig. 6 indicate a good correlation between the ratio of model-derived IN concentration and large aerosol concentration versus temperature. This is qualitatively similar to the trend seen in laboratory studies of desert dust acting as IN (e.g., Field et al. 2006b) and field compilations (DeMott et al. 2010) that included ICE-L data. These studies indicate that the fraction of aerosol that act as IN is reduced with increasing temperature. Taking the ratio of the measured IN counter concentrations (Table 2: IN concentrations processed at water saturation) to flight average UHSAS aerosol particle concentrations in the 0.5–1-μm range (as discussed in section 2) provides good agreement with the ratio derived from this modeling study (Fig. 6). This is encouraging because the IN counter often processed the aerosol at different temperatures than those observed in the lee wave cloud. Dividing Eq. (1) through by the aerosol concentration N_a from Table 1 leads to

$$\frac{N_{\text{in}}(T)}{N_a} = \frac{N_{\text{in0}}}{N_a}\exp(-BT^*), \tag{4}$$

where N_{in0}/N_a has a geometric mean and standard deviation of 0.06 and 0.36, respectively, for $B = 0.2$. Repeating the simulations and analysis with $B = 0.4$ results in N_{in0}/N_a having a geometric mean and standard deviation of 0.37 and 0.44, respectively. These two relations produce IN concentrations to within a factor of 2 between temperatures of −30° and −25°C, the temperature range that contains the majority of the data. The geometric standard deviation for $B = 0.2$ is only slightly

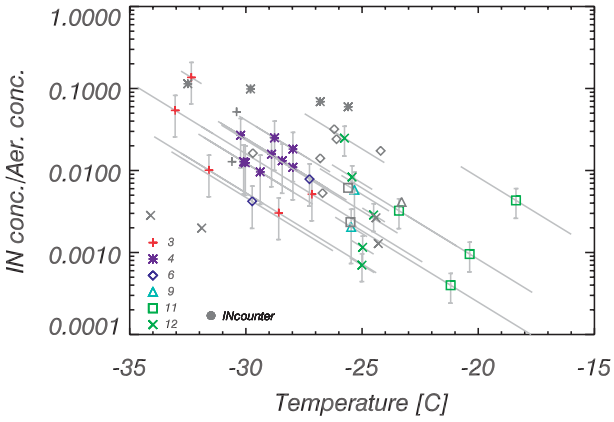

FIG. 7. As in Fig. 6, but for $B = 0.4$.

smaller than for $B = 0.4$, providing only marginal evidence for preferring $B = 0.2$. However, comparison of individual flights within Figs. 6 and 7 (e.g., flights 3 and 4) does suggest that $B = 0.2$ provides a tighter collapse of the data.

Using $B = 0.0$ and eliminating the temperature dependence also gives results that fall within the scatter exhibited in Fig. 6 (not shown). This is because the typical temperature range given in Table 1 for the freezing (~5°C) equates to a change in N_{in} of a factor of about 3. Because this range is comparable with the resolution of the N_{in0} values that were trialed, it explains why even removing the temperature dependence for individual runs produces similar results to those with nonzero B settings. To improve the choice of B, additional data are required, particularly at temperatures warmer than −20°C.

The variability in the relationship between aerosol concentrations of particles larger than 0.5 μm and IN concentrations for a given temperature is most likely due to variations in IN chemical composition (DeMott et al. 2010). To gain an understanding of the likely sources of cloud condensation nuclei (CCN) and IN influencing the lee wave clouds, the chemical composition of CVI residues and aerosol particles out of cloud was measured in real time using a single-particle mass spectrometer for the periods presented in this paper. During research flights 3 and 4, the majority of the cloud residues were identified as dry lakebed (playa) dust, characterized by salts composed of sodium, potassium, magnesium, and chloride (Pratt et al. 2010b). Playa dust containing silicates was most abundant among the cloud ice residues and was hypothesized to be important for heterogeneous ice nucleation (Pratt et al. 2010b), as observed in previous laboratory studies (Koehler et al. 2007). In contrast, research flights 6, 9, and 12 were primarily influenced by aged biomass burning (Pratt et al. 2010a). Minor fractions of mineral dust have been previously observed to be lofted during wildfires (Li et al. 2003); however, measurements are still needed to isolate the specific composition of IN within biomass burning plumes, which have been identified as sources of IN (Petters et al. 2009; Pratt et al. 2011; Twohy et al. 2010). Finally, research flight 11 was characterized by a variety of particle sources. Out of cloud the majority of the particles were from biomass burning, whereas the cloud residues were characterized primarily by biological particles (characterized by internally mixed organic carbon, potassium/sodium, phosphate, and often nitrate) and aged salts (sodium, potassium, chloride, nitrate, and sulfate). Thus, the sources, and therefore chemistry, of the particles influencing cloud nucleation varied significantly for these six flights. Because of the extremely low concentrations of IN, additional measurements of the chemical composition of ice particle residuals and of particles activated within IN counters will improve our understanding of the role of chemistry in ice nucleation.

6. Conclusions

Lee wave cloud penetrations by aircraft during the ICE-L field campaign have been combined with detailed 1D modeling to infer ice nucleation characteristics that can be beneficial for a heterogeneous ice nucleation parameterization to possess, and determine IN concentrations. Isolated lee wave clouds provide dynamically and thermodynamically constrained observational and modeling test beds for trialing microphysical packages.

Following a singular approach to heterogeneous nucleation, and based on the simple representations used here acting independently, the main ice production mechanism for these lee wave cloud observations was through condensation/immersion droplet freezing. Deposition or evaporation freezing alone could not reproduce the observed ice profiles. A correlation was seen between the ratio of model-derived IN concentrations and aerosol concentrations in the 500-nm–1-μm size range and temperature. We note that larger aerosol may also be important but 1000 nm is the large size limit of the UHSAS. It is thought that these large aerosols dominate as IN or at least contribute in greater proportion than smaller particles that are present in higher concentrations. Mineral dust is suggested as a major source of large aerosols acting as IN; however, additional measurements are needed to investigate other sources and the full size distribution of atmospheric IN.

The results imply that IN, especially those in the larger-aerosol ($D > 500$ nm) size range become increasingly more active with decreasing temperature. This behavior is both qualitatively and broadly quantitatively in agreement with the IN concentrations obtained from the IN counter.

Acknowledgments. We thank NCAR RAF for their support and dedication to the ICE-L project. The U.S. National Science Foundation (NSF) sponsored the ICE-L project, and the National Center for Atmospheric Research is supported by the NSF. P. J. DeMott acknowledges NSF for support during ICE-L (ATM0611936). K. A. Pratt and K. A. Prather acknowledge NSF for support (ATM-0650659). K. A. Pratt also acknowledges funding from an NSF Graduate Research Fellowship and a NOAA Climate and Global Change Postdoctoral Fellowship.

REFERENCES

Ansmann, A., and Coauthors, 2008: Influence of Saharan dust on cloud glaciation in southern Morocco during the Saharan Mineral Dust Experiment. *J. Geophys. Res.,* **113,** D04210, doi:10.1029/2007JD008785.

Baker, B. A., and R. P. Lawson, 2006: In situ observations of the microphysical properties of wave, cirrus, and anvil clouds. Part I: Wave clouds. *J. Atmos. Sci.,* **63,** 3160–3185.

Connolly, P. J., O. Möhler, P. R. Field, H. Saathoff, R. Burgess, T. Choularton, and M. Gallagher, 2009: Studies of heterogeneous freezing by three different desert dust samples. *Atmos. Chem. Phys.,* **9,** 2805–2824.

Cooper, W. A., 1986: Ice initiation in natural clouds. *Precipitation Enhancement—A Scientific Challenge, Meteor. Monogr.,* No. 43, Amer. Meteor. Soc., 29–32.

——, 1995: Ice formation in wave clouds: Observed enhancement during evaporation. Preprints, *Conf. on Cloud Physics,* Dallas, TX, Amer. Meteor. Soc., 147–152.

——, and G. Vali, 1981: The origin of ice in mountain cap clouds. *J. Atmos. Sci.,* **38,** 1244–1259.

Cotton, R. J., and P. R. Field, 2002: Ice nucleation characteristics of an isolated wave cloud. *Quart. J. Roy. Meteor. Soc.,* **128,** 2417–2437.

DeMott, P. J., D. C. Rogers, S. M. Kreidenweis, Y. Chen, C. H. Twohy, D. Baumgardner, A. J. Heymsfield, and K. R. Chan, 1998: The role of heterogeneous freezing nucleation in upper tropospheric clouds: Inferences from SUCCESS. *Geophys. Res. Lett.,* **25,** 1387–1390.

——, and Coauthors, 2003a: Measurements of the concentration and composition of nuclei for cirrus formation. *Proc. Natl. Acad. Sci. USA,* **100,** 14 655–14 660.

——, K. Sassen, M. R. Poellot, D. Baumgardner, D. C. Rogers, S. D. Brooks, A. J. Prenni, and S. M. Kreidenweis, 2003b: African dust aerosols as atmospheric ice nuclei. *Geophys. Res. Lett.,* **30,** 1732, doi:10.1029/2003GL017410L07808; Corrigendum, **36,** L07808, doi:10.1029/2009GL037639.

——, and Coauthors, 2010: Predicting global atmospheric ice nuclei distributions and their impacts on climate. *Proc. Natl. Acad. Sci. USA,* **107,** 11 217–11 222.

Durant, A. J., and R. A. Shaw, 2005: Evaporation freezing by contact nucleation inside-out. *Geophys. Res. Lett.,* **32,** L20814, doi:10.1029/2005GL024175.

Eidhammer, T., P. J. DeMott, and S. M. Kreidenweis, 2009: A comparison of heterogeneous ice nucleation parameterizations using a parcel model framework. *J. Geophys. Res.,* **114,** D06202, doi:10.1029/2008JD011095.

——, and Coauthors, 2010: Ice initiation by aerosol particles: Measured and predicted ice nuclei concentrations versus measured ice crystal concentrations in an orographic wave cloud. *J. Atmos. Sci.,* **67,** 2437–2450.

Field, P. R., and Coauthors, 2001: Ice nucleation in orographic wave clouds: Measurements made during INTACC. *Quart. J. Roy. Meteor. Soc.,* **127,** 1493–1512.

——, A. J. Heymsfield, and A. Bansemer, 2006a: Shattering and particle interarrival times measured by optical array probes in ice cloud. *J. Atmos. Oceanic Technol.,* **23,** 1357–1371.

——, O. Möhler, P. Connolly, M. Krämer, R. Cotton, A. J. Heymsfield, H. Saathoff, and M. Schnaiter, 2006b: Some ice nucleation characteristics of Asian and Saharan desert dust. *Atmos. Chem. Phys.,* **6,** 2991–3006.

Hallett, J., 1968: Nucleation and growth of ice crystals in water and biological systems. *Low Temperature Biology of Foodstuffs,* J. Hawthorne, Ed., Pergamon Press, 29–32.

Heymsfield, A. J., and L. M. Miloshevich, 1993: Homogeneous ice nucleation and supercooled liquid water in orographic wave clouds. *J. Atmos. Sci.,* **50,** 2335–2353.

——, and ——, 1995: Relative humidity and temperature influences on cirrus formation and evolution: Observations from wave clouds and FIRE II. *J. Atmos. Sci.,* **52,** 4302–4326.

——, P. R. Field, M. Bailey, D. C. Rogers, J. Stith, C. Twohy, Z. Wang, and S. Haimov, 2011: Ice in Clouds Experiment–Layer Clouds. Part I: Ice growth rates derived from lenticular wave cloud penetrations. *J. Atmos. Sci.,* **68,** 2628–2654.

Jensen, E. J., and Coauthors, 1998: Ice nucleation processes in upper tropospheric wave-clouds observed during SUCCESS. *Geophys. Res. Lett.,* **25,** 1363–1366.

Knollenberg, R. G., 1970: The optical array: An alternative to extinction and scattering for particle size measurements. *J. Appl. Meteor.,* **9,** 86–103.

Koehler, K. A., S. M. Kreidenweis, P. J. DeMott, A. J. Prenni, and M. D. Petters, 2007: Potential impact of Owens (dry) Lake dust on warm and cold cloud formation. *J. Geophys. Res.,* **112,** D12210, doi:10.1029/2007JD008413.

Leonard, B. P., M. K. MacVean, and A. P. Lock, 1993: Positivity-preserving numerical schemes for multidimensional advection. NASA Tech. Memo. 106055 (ICOMP-93905), 62 pp.

Li, J., M. Pósfai, P. V. Hobbs, and P. R. Buseck, 2003: Individual aerosol particles from biomass burning in southern Africa: 2. Compositions and aging of inorganic particles. *J. Geophys. Res.,* **108,** 8484, doi:10.1029/2002JD002310.

Mason, B. J., 1950: The nature of ice-forming nuclei in the atmosphere. *Quart. J. Roy. Meteor. Soc.,* **76,** 59–74.

Meyers, M. P., P. J. DeMott, and W. R. Cotton, 1992: New primary ice-nucleation parameterizations in an explicit cloud model. *J. Appl. Meteor.,* **31,** 708–721.

Möhler, O., and Coauthors, 2006: Efficiency of the deposition mode ice nucleation on mineral dust particles. *Atmos. Chem. Phys.,* **6,** 3007–3021.

Murray, B. J., S. L. Broadley, T. W. Wilson, J. D. Atkinson, and R. H. Wills, 2011: Heterogeneous freezing of water droplets containing kaolinite particles. *Atmos. Chem. Phys.,* **11,** 4191–4207.

Niedermeier, D., R. A. Shaw, S. Hartmann, H. Wex, T. Clauss, J. Voigtländer, and F. Stratmann, 2011: Heterogeneous ice nucleation: Exploring the transition from stochastic to singular freezing behavior. *Atmos. Chem. Phys.,* **11,** 8767–8775, doi:10.5194/acp-11-8767-2011.

Petters, M. D., and Coauthors, 2009: Ice nuclei emissions from biomass burning. *J. Geophys. Res.,* **114,** D07209, doi:10.1029/2008JD011532.

Phillips, V. T. J., P. J. DeMott, and C. Andronache, 2008: An empirical parameterization of heterogeneous ice nucleation for multiple chemical species of aerosol. *J. Atmos. Sci.,* **65,** 2757–2783.

Pratt, K. A., and Coauthors, 2009: Development and characterization of an aircraft aerosol time-of-flight mass spectrometer. *Anal. Chem.,* **81,** 1792–1800.

——, and Coauthors, 2010a: In situ chemical characterization of aged biomass-burning aerosols impacting cold wave clouds. *J. Atmos. Sci.,* **67,** 2451–2468.

——, and Coauthors, 2010b: Observation of playa salts as nuclei in orographic wave clouds. *J. Geophys. Res.,* **115,** D15301, doi:10.1029/2009JD013606.

——, and Coauthors, 2011: Flight-based chemical characterization of biomass burning aerosols within two prescribed burn smoke plumes. *Atmos. Chem. Phys. Discuss.,* **11,** 17 507–17 550.

Richardson, M. S., and Coauthors, 2007: Measurements of heterogeneous ice nuclei in the western United States in springtime and their relation to aerosol characteristics. *J. Geophys. Res.,* **112,** D02209, doi:10.1029/2006JD007500.

Rogers, D. C., P. J. DeMott, S. M. Kreidenweis, and Y. Chen, 2001: A continuous-flow diffusion chamber for airborne measurements of ice nuclei. *J. Atmos. Oceanic Technol.,* **18,** 725–741.

Rosinski, J., and G. Morgan, 1991: Cloud condensation nuclei as a source of ice-forming nuclei in clouds. *J. Aerosol Sci.,* **22,** 123–133.

Ryan, B. E., E. R. Wishart, and D. E. Shaw, 1976: The growth rates and densities of ice crystals between 3° and 21°C. *J. Atmos. Sci.,* **33,** 842–850.

Shipway, B. J., and A. A. Hill, 2012: Diagnosis of systematic differences between multiple parametrizations of warm rain microphysics using a kinematic framework. *Quart J. Roy. Meteor. Soc.,* in press.

Stith, J. L., and Coauthors, 2009: An overview of aircraft observations from the Pacific Dust Experiment campaign. *J. Geophys. Res.,* **114,** D05207, doi:10.1029/2008JD010924.

Strapp, J. W., F. Albers, A. Reuter, A. V. Korolev, U. Maixner, E. Rashke, and Z. Vukovic, 2001: Laboratory measurements of the response of a PMS OAP-2DC. *J. Atmos. Oceanic Technol.,* **18,** 1150–1170.

Swann, H., 1998. Sensitivity to the representation of precipitating ice in CRM simulations of deep convection. *Atmos. Res.,* **48,** 415–435.

Takahashi, T., T. Endoh, G. Wakahama, and N. Fukuta, 1991: Vapor diffusional growth of free-falling snow crystals between 3° and 23°C. *J. Meteor. Soc. Japan,* **69,** 15–30.

Twohy, C. H., A. J. Schanot, and W. A. Cooper, 1997: Measurement of condensed water content in liquid and ice clouds using an airborne counterflow virtual impactor. *J. Atmos. Oceanic Technol.,* **14,** 197–202.

——, and Coauthors, 2010: Relationships of biomass-burning aerosols to ice in orographic wave clouds. *J. Atmos. Sci.,* **67,** 2437–2450.

Vali, G., 1994: Freezing rate due to heterogeneous nucleation. *J. Atmos. Sci.,* **51,** 1843–1856.

Young, K. C., 1974: The role of contact nucleation in ice phase initiation in clouds. *J. Atmos. Sci.,* **31,** 768–776.